Mon. Not. R. Astron. Soc. **000**, 1–10 (0000) Printed 5 October 2012 (MN LaTeX style file v2.2)

arXiv:1210.1483v1 [astro-ph.CO] 4 Oct 2012

Excursion set peaks: a self-consistent model of dark halo abundances and clustering

Aseem Paranjape[1]*, Ravi K. Sheth[1,2]† & Vincent Desjacques[3]‡
[1] *The Abdus Salam International Center for Theoretical Physics, Strada Costiera, 11, Trieste 34151, Italy*
[2] *Center for Particle Cosmology, University of Pennsylvania, 209 S. 33rd St., Philadelphia, PA 19104, USA*
[3] *Département de Physique Théorique and Center for Astroparticle Physics (CAP) Université de Genève,*
24 quai Ernest Ansermet, CH-1211 Genève, Switzerland

5 October 2012

ABSTRACT

We describe how to extend the excursion set peaks framework so that its predictions of dark halo abundances and clustering can be compared directly with simulations. These extensions include: a halo mass definition which uses the TopHat filter in real space; the mean dependence of the critical density for collapse $\delta_{\rm c}$ on halo mass m; and the scatter around this mean value. All three of these are motivated by the physics of triaxial rather than spherical collapse. A comparison of the resulting mass function with N-body results shows that, if one uses $\delta_{\rm c}(m)$ and its scatter as determined from simulations, then all three are necessary ingredients for obtaining $\sim 10\%$ accuracy. E.g., assuming a constant value of $\delta_{\rm c}$ with no scatter, as motivated by the physics of spherical collapse, leads to many more massive halos than seen in simulations. The same model is also in excellent agreement with N-body results for the linear halo bias, especially at the high mass end where the traditional peak-background split argument applied to the mass function fit is known to underpredict the measured bias by $\sim 10\%$. In the excursion set language, our model is about walks centered on special positions (peaks) in the initial conditions – we discuss what it implies for the usual calculation in which all walks contribute to the statistics.

Key words: large-scale structure of Universe

1 INTRODUCTION

The evolution of the abundance of virialized clusters is a powerful probe of the combined effects of the nature of the initial conditions (Gaussian or not?), the nature of gravity (general relativity or not?), and the expansion history of the Universe (cosmological constant or more complex?). This has motivated studies to understand and parametrize this dependence, so that datasets can more precisely constrain the physical models.

There are three widespread approaches to modeling cluster abundances. The most accurate of these is the brute force numerical simulation method; one simply asserts that the dark matter halos which form in these simulations represent clusters in the Universe. However, this method is computationally expensive owing to the nonlinear nature of gravitational structure formation. The other two are simpler analytic models which consider the statistics of the initial fluctuation field to model halo formation. One is based on peaks, and attempts to model the comoving number density dn/dm of objects of a given mass m (Bardeen et al., 1986; Appel & Jones, 1990; Manrique et al., 1998; Hanami, 2001). The other, known as the excursion set approach, seeks to count the mass fraction $f(m)$ that is bound-up in objects of a given mass, and, from this, to infer the abundances of objects themselves (Press & Schechter, 1974; Peacock & Heavens, 1990; Bond et al., 1991; Sheth & Tormen, 2002; Maggiore & Riotto, 2010a; Musso & Sheth, 2012). The two are related by the simple fact that mass weighting each halo must yield the

---

* Current address: ETH Zürich, Instt. for Astronomy, Wolfgang-Pauli-Strasse 27, CH-8093 Zürich, Switzerland;
E-mail: aseemp@phys.ethz.ch
† E-mail: sheth@ictp.it
‡ E-mail: Vincent.Desjacques@unige.ch

© 0000 RAS

mass fraction in halos, so

$$\int_M^\infty \mathrm{d}m\,\frac{\mathrm{d}n(m)}{\mathrm{d}m}\,m = \bar\rho\int_M^\infty f(m)\,\mathrm{d}m. \qquad (1)$$

However, this subtle difference has led to rather different formulations of the problem. Only recently have the two approaches been written in the same formalism (Paranjape & Sheth, 2012), allowing a direct comparison of how they differ. Whereas all previous excursion set calculations of f were based on the statistics of *all* positions in the initial density fluctuation field, Paranjape & Sheth (2012) showed that the Excursion Set Peaks (ESP) calculation of f explicitly uses the statistics of a small subset of positions in the initial field (those associated with peaks).

Working with a special subset of positions is motivated by measurements extracted from simulations showing that the excursion set prediction for the mass of the object in which a randomly chosen particle ends up is almost always incorrect (White, 1996), whereas the prediction for the subset of particles which are at the center of mass of the proto-halo is almost always quite accurate (Sheth, Mo & Tormen, 2001). Moreover, for this special subset of (center-of-mass) particles, the predicted mass depends on whether one assumes a spherical or a triaxial collapse – and the prediction is more accurate if one uses the more physically appropriate (though by no means perfect!) triaxial collapse model. In other words, the physics and the statistics are simpler, and tell a consistent story only if one works directly with the special subset of positions around which collapse occurs. More recent work has shown that proto-halo positions do indeed coincide with peaks in the initial field (Ludlow & Porciani, 2011), and their initial velocities are biased with respect to that of the dark matter (Elia, Ludlow & Porciani, 2012), as is expected for peaks (Desjacques & Sheth, 2010). This provides additional motivation for the ESP approach.

However, this approach raises the following technical problem. The peaks approach uses the statistics of the smoothed density field, as well as its first and second derivatives. As a result, the rms values of these quantities play an important role. In the theory, these rms values are related to integrals over the initial power spectrum. However, they depend on the form of the smoothing filter, and, for the TopHat smoothing filter which is expected to be most directly related to the physics of gravitational collapse, some of these integrals do not converge. For Gaussian filters there is no such problem, and Paranjape & Sheth (2012) showed that, when expressed in suitably scaled (and natural) units ν, the ESP prediction for halo abundances is in excellent agreement with simulations, when the measured halo abundances are also expressed in scaled units. Namely, if one sets

$$\frac{m}{\bar\rho}\frac{\mathrm{d}n(m)}{\mathrm{d}\ln m} = \nu\, f(\nu)\,\left|\frac{\mathrm{d}\ln\nu}{\mathrm{d}\ln m}\right|, \qquad (2)$$

then the ESP $\nu f(\nu)$ is in good agreement with the distribution of $\ln\nu$ measured in simulations. However, this agreement is only a partial success because the relation between halo mass and ν depends on the smoothing filter, and the ESP model employed a Gaussian filter whereas simulations use a TopHat. Therefore, when expressed as a function of mass, the Gaussian smoothed ESP prediction is not a good description of $\mathrm{d}n/\mathrm{d}\ln m$ in simulations (because the Jacobian $d\ln\nu/d\ln m$ depends on the filtering kernel). Moreover, the Gaussian ESP prediction assumed that halos form through a spherical collapse, even though this is an incorrect description of the physics of halo formation (Sheth et al., 2001). In fact, there is substantial scatter even in the triaxial collapse model (Sheth et al., 2001; Sheth, 2009; Dalal et al., 2008; Robertson et al., 2009; Ludlow & Porciani, 2011), so the latter also provides an incomplete description of collapse. There has been some discussion of how to include stochasticity into the predictions (Bond & Myers, 1996; Chiueh & Lee, 2001; Sheth & Tormen, 2002; Desjacques, 2008; Maggiore & Riotto, 2010b; Corasaniti & Achitouv, 2011; Paranjape, Lam & Sheth, 2012; Sheth, Chan & Scoccimarro, 2012), but none of these self-consistently combines the model for the stochasticity with the fact that estimates of this stochasticity, from simulations or from theory, are for the special subset of positions around which collapse occurs.

Therefore, the main goals of the present work are to include TopHat smoothing in the ESP formalism and incorporate the effects of more complicated collapse models which are seen in simulations. All this is the subject of Section 2. Some testable predictions which elucidate the relation between the ESP approach and the usual excursion set analysis of all (rather than special) positions in space are discussed in Section 3. Section 4 presents implications for the spatial distribution of these objects – the ESP predictions for Lagrangian halo bias – which can be used to further test the model. A final section summarizes our results. We will show numerical results at redshift $z = 0$ for two ΛCDM cosmologies: one with $(\Omega_m, \Omega_\Lambda, \sigma_8, n_s, h) = (0.3, 0.7, 0.9, 1.0, 0.7)$ which we denote WMAP1 and the other with $(0.25, 0.75, 0.8, 1.0, 0.7)$ which we denote WMAP3.

2 THE UNCONDITIONAL MASS FUNCTION

2.1 Notation

We will designate Gaussian filtered quantities with the subscript G. By contrast, TopHat filtered objects will have no subscript. The Fourier transforms of the TopHat and Gaussian filters are $W(kR) = (3/kR)j_1(kR)$ and $W_{\rm G}(kR_{\rm G}) = \mathrm{e}^{-k^2R_{\rm G}^2/2}$, respectively, with $j_1(y)$ a spherical Bessel function.

We will frequently need the following integrals over the linearly extrapolated dimensionless matter power spectrum $\Delta^2(k) \equiv k^3P(k)/2\pi^2$:

TopHat-filtered variance:

$$s \equiv \sigma_0^2 \equiv \langle\,\delta^2\,\rangle = \int \mathrm{d}\ln k\,\Delta^2(k)W(kR)^2\,. \qquad (3)$$

We will exclusively use the notation $\nu \equiv \delta_c/\sigma_0$ where $\delta_c = 1.686$ is the usual spherical collapse threshold.

Gaussian-filtered spatial moments:

$$\sigma^2_{j\mathrm{G}} \equiv \int \mathrm{d}\ln k\, \Delta^2(k)\, k^{2j} W_{\mathrm{G}}(kR_{\mathrm{G}})^2 \quad, \; j \geq 1\,, \tag{4}$$

so that $\sigma^2_{1\mathrm{G}} = \langle\, (\nabla\delta_{\mathrm{G}})^2\,\rangle$ and $\sigma^2_{2\mathrm{G}} = \langle\, (\nabla^2\delta_{\mathrm{G}})^2\,\rangle$.

Mixed moment:

$$\begin{aligned}\sigma^2_{1\mathrm{m}} &\equiv \langle\, -\delta\,\nabla^2\delta_{\mathrm{G}}\,\rangle \\ &= \int \mathrm{d}\ln k\, \Delta^2(k)\, k^2 W_{\mathrm{G}}(kR_{\mathrm{G}}) W(kR)\,. \end{aligned} \tag{5}$$

Characteristic volume:

$$R_* \equiv \sqrt{3}\sigma_{1\mathrm{G}}/\sigma_{2\mathrm{G}} \qquad ; \qquad V_* = (2\pi)^{3/2} R_*^3\,. \tag{6}$$

These are the same as defined by Bardeen et al. (1986).

Spectral parameter:

$$\gamma \equiv \frac{\sigma^2_{1\mathrm{m}}}{\sigma_0\sigma_{2\mathrm{G}}} = \frac{\langle\, -\delta\,\nabla^2\delta_{\mathrm{G}}\,\rangle}{\sqrt{\langle\, \delta^2\,\rangle\,\langle\,(\nabla^2\delta_{\mathrm{G}})^2\,\rangle}} = \langle\, x\mu\,\rangle\ , \tag{7}$$

where we defined the standardised variables

$$\mu \equiv \delta/\sigma_0 \qquad \text{and} \qquad x \equiv -\nabla^2\delta_{\mathrm{G}}/\sigma_{2\mathrm{G}}\,. \tag{8}$$

Note that this definition of γ is similar but not identical to the corresponding one in Bardeen et al. (1986), since our peak heights are defined using TopHat smoothing.

2.2 Matching filter scales

The technical problem which we address in this subsection is how to ensure that the peaks in the Gaussian filtered density field δ_{G} will have an overdensity $\delta_{\mathrm{TH}} = \delta_c$ when smoothed with a TopHat, since essentially all measurements in simulations use TopHats only. In practice, we need a mapping between the scales R_{TH} and R_{G} of the two filters. All previous work accomplishes this either by matching the volumes: $(4\pi/3)\, R^3_{\mathrm{TH}} = (2\pi)^{3/2}\, R^3_{\mathrm{G}}$, or by matching the variances: $\langle\, \delta^2_{\mathrm{TH}}\,\rangle = \langle\, \delta^2_{\mathrm{G}}\,\rangle$. In this second case, the relation between R_{TH} and R_{G} depends on the shape of the power spectrum. But neither of these conditions guarantee that a peak identified on scale R_{G} satisfies $\delta_{\mathrm{TH}} = \delta_c$.

For this reason, we construct the mapping between R_{TH} and R_{G} by finding that R_{G} (at a given R_{TH}) for which $\langle\, \delta_{\mathrm{G}}|\delta_{\mathrm{TH}}\,\rangle = \delta_{\mathrm{TH}}$. This is equivalent to $\langle\, \delta_{\mathrm{G}}\delta_{\mathrm{TH}}\,\rangle = \langle\, \delta^2_{\mathrm{TH}}\,\rangle$. This definition circumvents the technical complication arising from the variance of the Laplacian of δ_{TH} (which involves a divergent integral). For the ΛCDM $P(k)$ we consider in this paper, $R_{\mathrm{G}} \approx 0.46 R_{\mathrm{TH}}$ with a mild mass-dependence which we account for, in the range we explore, $3 \times 10^{10} < m/(h^{-1}M_\odot) < 3 \times 10^{15}$.

Our choice of matching between R_{TH} and R_{G}, namely $\langle\, \delta_{\mathrm{G}}|\delta\,\rangle = \delta$, means that $p(\delta_{\mathrm{G}}|\delta)$ is a Gaussian with mean δ and variance $\langle\, \delta^2_{\mathrm{G}}\,\rangle - s$. However, $\langle\, \delta^2_{\mathrm{G}}\,\rangle \approx s$ to better than 5% and, thus, $p(\delta_{\mathrm{G}}|\delta) \approx \delta_{\mathrm{D}}(\delta_{\mathrm{G}} - \delta)$ (since the cross-correlation between δ_{G} and δ is very close to unity). This significantly simplifies our ESP analysis for the following reason. In principle, the excursion set peaks framework also requires us to keep track of the variable $\tilde{x} \equiv \delta'/\sqrt{\langle\, \delta'^2\,\rangle}$, where $\delta' = \mathrm{d}\delta/\mathrm{d}s$. This scalar (isotropic) variable correlates with μ and x, but not with the other (anisotropic) variables used by Bardeen et al. (1986). Therefore, one should in principle work with the three-dimensional Gaussian vector $(\mu, x, \tilde{x})$. However, because $p(\delta_{\mathrm{G}}|\delta) \approx \delta_{\mathrm{D}}(\delta_{\mathrm{G}} - \delta)$, it turns out that setting $\tilde{x} = x$ yields an excellent approximation (notice that this relation is exact for the Gaussian filter). We have indeed checked that our final answers for $dn/d\ln m$ only change by a few percent if we switch between the approximate and exact treatments. In the following, we will therefore always set $\tilde{x} = x$ and only work with the two-dimensional Gaussian vector (μ, x).

2.3 Excursion set peaks with a constant barrier

Apart from the fact that the peak height is defined using TopHat filtering, there is no formal change in the derivation by Paranjape & Sheth (2012) of the number density of excursion set peaks for a constant barrier (and this derivation is formally the same as that in Appel & Jones, 1990). In this case we get

$$\begin{aligned} f_{\mathrm{ESP}}(\nu) &= V\mathcal{N}_{\mathrm{ESP}}(\nu) \\ &= (V/V_*)(\mathrm{e}^{-\nu^2/2}/\sqrt{2\pi}) \\ &\qquad \times \int_0^\infty \mathrm{d}x\, \frac{x}{\gamma\nu}\, F(x) p_{\mathrm{G}}(x - \gamma\nu; 1 - \gamma^2)\,, \end{aligned} \tag{9}$$

where $V = m/\bar{\rho} = 4\pi R^3/3$ is the Lagrangian volume associated with the TopHat smoothing filter, $F(x)$ is the peak curvature function from equation (A15) of Bardeen et al. (1986) and $p_{\mathrm{G}}(y - \bar{y}; \Sigma^2)$ is a Gaussian distribution in y with mean $\bar{y}$ and variance Σ^2. (As noted in Paranjape & Sheth, 2012, $F(x) \neq 1$ reflects the fact that the ESP calculation averages over a special subset of positions.) Since we have been careful to define ν and hence the mass using TopHat filtering, the mass function follows in the usual way from equation (2).

Figure 1 compares the ESP result for a constant barrier $B(s) = \delta_c = 1.686$ (solid red) with the fit to N-body simulations from Tinker et al. (2008) (dashed green). For the latter we used parameters from Table 2 of Tinker et al. (2008) appropriate for halos identified using the spherical overdensity (SO) definition at 200 times the mean density of the universe. We used cosmological parameters for the WMAP1 cosmology mentioned in the Introduction, for which the Tinker et al. (2008) function gives a good fit (c.f. their Table 2). Later we will also show results for the WMAP3 cosmology which was also explored by Tinker et al. (2008) – changing cosmology does not affect our results significantly. For comparison we also show the Sheth & Tormen (1999) result (short-dashed blue) with their $(q, p) = (0.7, 0.26)$ which gives a good fit to the MICE simulations (Crocce et al., 2010).

Clearly, equation (9) predicts far too many halos at all interesting scales, including the high mass end

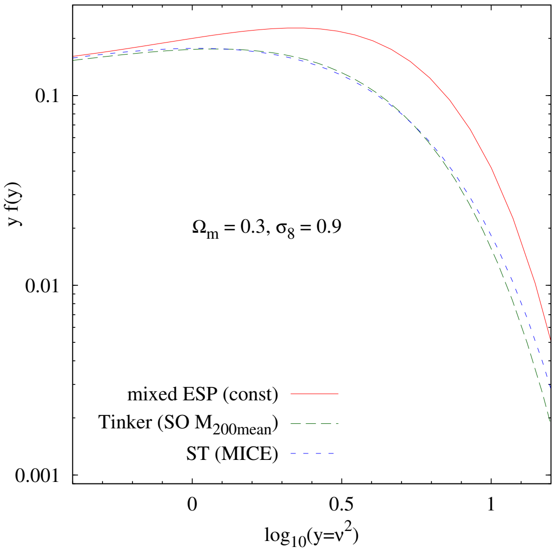

Figure 1. Excursion set peaks mass function for the mixed filtering approach discussed in the text, using a constant barrier (solid red). This is compared with the fit to N-body simulations given by Tinker et al. (2008), appropriate for spherical overdensity halos that enclose 200 times the mean density of the universe (dashed green). For comparison, we also show the Sheth & Tormen (1999) mass function (short-dashed blue) with their $(q, p) = (0.7, 0.26)$, which gives a good fit to the MICE simulations (Crocce et al., 2010). The ESP+constant barrier mass function overpredicts the abundance at all scales of interest. All curves used the WMAP1 cosmology – we have checked that changing the cosmology does not significantly alter the comparison.

($\nu^2 = 10$ corresponds to $m = 1.3 \times 10^{15} h^{-1} M_\odot$ for this cosmology).

2.4 Beyond the spherical-collapse constant barrier

It is tempting to attribute the mismatch shown in Figure 1 to the effects of non-spherical collapse. While these effects are certainly important at smaller mass scales, it is not obvious that they also matter at the largest scales, where the spherical collapse approximation should be quite accurate. To see that they are in fact relevant, note that the triaxial collapse model predicts that the critical density for collapse scales approximately as

$$\delta_{\rm ec} \approx \delta_{\rm c}[1 + 0.4(\sigma_0/\delta_{\rm c})^{1.2}] \qquad (10)$$

(Sheth et al., 2001). Simulations indeed show that this expression for $\delta_{\rm ec}$ provides a reasonable approximation to the mass dependence of the critical density required for collapse (Sheth et al., 2001). However, this implies that when $\nu = \delta_{\rm c}/\sigma_0$ is as large as ~ 4, then departures from the spherical $\delta_{\rm c}$ are already of the order of ten percent. Therefore, we must include deviations from the spherical collapse barrier in order to have a fair comparison with the Tinker et al. (2008) simulations.

Before explaining how this can be done, we note that, although equation (10) is a reasonable approximation to the mass dependence of the critical density required for collapse (Sheth et al., 2001), there is substantial scatter around this value (Sheth, 2009). This scatter has been quantified by Robertson et al. (2009) who approximated $\delta_{\rm ec}$ by[1]

$$B = \delta_{\rm c} + \beta\sqrt{s} \qquad (11)$$

and found that, over the range $\log_{10}(\nu^2) \in (-0.3, 0.9)$, the value of B was Lognormally distributed around a mean value of $\simeq \delta_{\rm c} + 0.43\sigma_0$ with variance $(0.09\sigma_0^2)$. The physical origin of this scatter is unclear. Triaxial collapse predicts some scatter (Sheth et al., 2001), which is related to the statistics of the tidal field, but the measured scatter is considerably larger. In any case, the physical origin of this scatter is unimportant for what follows - though we believe that this is an issue which deserves further investigation.

2.5 Excursion set peaks with a square-root barrier and scatter

To include the mean trend and scatter in barrier heights shown by Sheth et al. (2001) and quantified by Robertson et al. (2009), we will adopt the following model, first discussed in Paranjape et al. (2012). We consider a family of deterministic "square-root" barriers B given by equation (11), with β a stochastic variable. Therefore, if $f_{\rm ESP}(\nu|\beta)$ denotes the ESP solution for a given value of β, then our full solution will be

$$f_{\rm ESP}(\nu) = \int {\rm d}\beta\, p(\beta)\, f_{\rm ESP}(\nu|\beta). \qquad (12)$$

Below we use simulations to motivate our choice of $p(\beta)$, and provide an explicit expression for $f_{\rm ESP}(\nu|\beta)$. Still, it is easy to understand qualitatively what happens.

For excursion set peaks, the square root barrier (11) with $\beta > 0$ dramatically lowers the halo counts at large masses (Figure 3 in Paranjape & Sheth, 2012). While this goes in the right direction, introducing scatter in the value of β will counteract this decrease. This is because a scatter in β induces a scatter in the predicted mass of the halo. The steepness of the mass function implies that the scatter preferentially moves small mass objects to larger masses (the same effect that leads to Eddington bias), which in turn increases the abundance at large masses.

The importance of the scatter depends on the distribution of β. Our choice for $p(\beta)$ is particularly simple. As discussed in the previous section, the distribution of

---

[1] We use the results of Robertson et al. (2009) rather than those of Dalal et al. (2008) because the latter only show a plot whereas Robertson et al. provide a fit to a probability distribution. Both groups find a similar mean and r.m.s. for the barrier heights, however, which increase approximately linearly with σ_0.

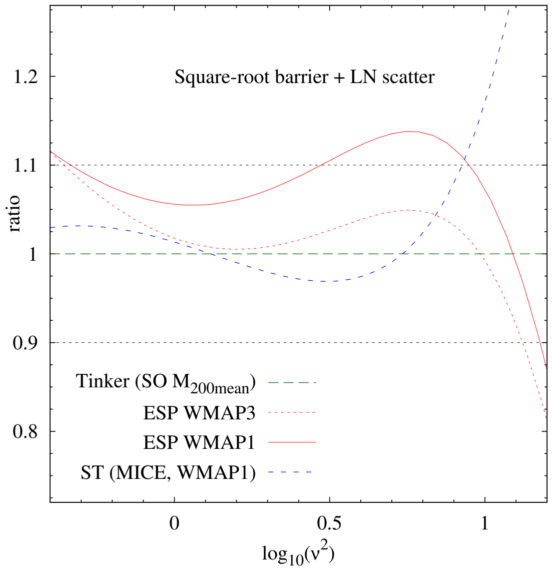

Figure 2. Ratio of the ESP mass function for a square-root barrier with scatter in the barrier slope (equation 12) to the Tinker et al. (2008) fit, for WMAP1 (solid red) and WMAP3 (dotted red) cosmologies. In each case we set $\delta_c = 1.686$ and $p(\beta)$ to be Lognormal with $\langle\, \beta\, \rangle = 0.43$ and $\sqrt{\mathrm{Var}(\beta)} = 0.3$, for the reasons discussed in the text. For comparison we also show the ratio of the MICE fit with the Tinker et al. fit for the WMAP1 cosmology (short-dashed blue). Horizontal dotted lines mark 10% deviations from the Tinker et al. fit, which is the typical scatter in their measurements in this mass range.

B seen in simulations for halos of a fixed mass is Lognormal, so we choose the distribution of β to be Lognormal with $\langle\, \beta\, \rangle = 0.43$ and $\mathrm{Var}(\beta) = 0.09$.

For square-root barriers with fixed β (equation 19 of Paranjape & Sheth, 2012, for the barrier in equation 11 above),

$$f_{\mathrm{ESP}}(\nu|\beta) = (V/V_*)(\mathrm{e}^{-(\nu+\beta)^2/2}/\sqrt{2\pi}) \times \int_{\beta\gamma}^{\infty} \mathrm{d}x\, \frac{x-\beta\gamma}{\gamma\nu} F(x) \times p_{\mathrm{G}}(x-\beta\gamma-\gamma\nu; 1-\gamma^2)\,. \quad (13)$$

We have assumed $\beta > 0$, which is true for the Lognormal model we will consider. If β is allowed to take negative values as well, then the lower limit of the integral over x must be replaced by $x_{\min} = \max\{0, \beta\gamma\}$, so as to enforce the peak constraint. While there is no closed form expression for $f_{\mathrm{ESP}}(\nu)$, the integrals involved can be easily computed numerically. Note that, because we use the distribution $p(\beta)$ that is seen in simulations, our model has *no* free parameters.

Figure 2 shows the results for the WMAP1 (solid red) and WMAP3 (dotted red) cosmologies. Note that the value of σ_8 is $\sim$ 10% smaller in the WMAP3 cosmology. We plot the ratio of the ESP prediction in equation (12) and the Tinker et al. (2008) fit. For comparison we also indicate the ratio of the MICE fit with the Tinker et al. fit (for the WMAP1 cosmology) as the short-dashed blue curve. The horizontal dotted lines mark 10% deviations from the Tinker et al. fit, which is the typical scatter in their measurements in this mass range (c.f. figure 6a of Tinker et al., 2008). This shows that our model, which has no free parameters, works rather well.

3 IMPLICATIONS FOR AVERAGES OVER ALL, RATHER THAN A SPECIAL SUBSET OF POSITIONS

The ESP model of the previous section is the first to self-consistently integrate the complex physics of non-spherical collapse with the fact that the physics is almost certainly simplest around the center-of-mass of the proto-halo. Although the agreement with the halo counts represents a significant and nontrivial success, and the next section shows that the predicted spatial distribution is also accurate, it makes a number of other testable predictions which are related to the logic of the excursion set approach.

For example, one can construct the center-of-mass random walk associated with each halo and explicitly check, object by object, whether or not the corresponding barrier was crossed at a larger scale. This is, in fact, precisely the kind of test which was performed by Sheth et al. (2001). Revisiting this test is left to future work.

3.1 Distribution of δ for all particles in proto-halos of a given mass

We remarked in the Introduction that our ESP model explicitly averages only over special positions in the universe (see text following equation 9 for exactly where this happens). If we treat these positions as the fundamental quantities (for which the physics of collapse is most easily applied), then by accounting for their initial density profiles, it is straightforward to estimate what would have happened had we averaged over all positions. Because our model has been calibrated for center of mass positions solely, predicting the right distribution of δ values within each proto-halo provides another test of our approach. We sketch the idea below.

We begin with noting that the distribution of δ at distance r from a peak is a Gaussian with mean approximately given by $\sigma\,(\nu - \gamma\,\langle\, x|\nu\,\rangle)/(1-\gamma^2)\,\xi(r)/\xi(0)$ and variance approximately $\sigma^2\left[1 - (\xi(r)/\xi(0))^2/(1-\gamma^2)\right]$ (equations 7.8–7.10 in Bardeen et al., 1986). Note that the mean value asymptotes to $\sigma\nu\,\xi(r)/\xi(0)$ in the limit $\nu \gg 1$. Since $\xi(r) < \xi(0)$, the term $\xi(r)/\xi(0) \equiv \Xi$ is the ratio by which the density at r drops from its value at the center.

In our model, at any given mass scale there is a distribution of δ values for the special positions around which collapse occurs; call these values δ_{pk}. This distribution has a variance, say, $\sigma^2\Sigma^2_\beta$. And, for each δ_{pk}, there is a Gaussian distribution of δ for any position at a distance

$r < R$ from the center (the one just described above). Since all these have the same variance, the result of averaging over the r-shells yields a distribution with variance σ^2 times $1 - \Xi^2/(1-\gamma^2) + \Xi^2\,\Sigma_\beta^2$.

The shape of this distribution should still be approximately Gaussian if $\Sigma_\beta^2 \ll 1 - \Xi^2/(1-\gamma^2)$. This should indeed be the case; we know that $\gamma \approx 1/2$ and $\Sigma_\beta \approx 1/3$, and we can reasonably assume $1/2 < \Xi < 1$, with Ξ not being very close to unity (since we average over r-shells that are within one smoothing radius of the halo center of mass, and the shells near $r = 0$ contribute little to the total volume). Consequently, the expected distribution of δ, measured by looking at all positions within protohalos of mass $m(\sigma^2)$ (i.e. not only those corresponding to the proto-halo centers of mass) is a Gaussian whose mean value is a factor $1/2 < \Xi < 1$ smaller than that associated with the physics of collapse, and whose variance is $\approx \sigma^2\,(1 - 1.25\,\Xi^2)$. For example, if $\Xi = 3/4$ then the variance should be $\approx 0.3\sigma^2$. This dependence on σ, as well as the fact that Ξ appears both in the expression for the mean δ as well as its variance, are both testable, as is the prediction that the shape should be well approximated by a Gaussian, even though the distribution of $\delta_{\rm pk}$ is not.

3.2 Distribution of predicted mass for all particles in proto-halos of a given mass

The lower mean value implies that the mass which the excursion set approach predicts for the particles which are not at the center of mass should be systematically smaller than the mass of the halo in which they end up – in qualitative agreement with one of the findings of Sheth et al. (2001, see their Figures 2-4).

To see that this is indeed the case, we can use our ESP approach (walks centered on peaks in the initial field) to model what the usual excursion set estimate (walks centered on all positions in the initial field) really represents. Recall that, for the statistics of all positions, we know that if $\delta_{\rm c}$ is independent of m then the excursion set prediction for the mass fraction in objects with mass $m(s)$ is $sf(s) = \nu\,\exp(-\nu^2/2)/\sqrt{2\pi}$ with $\nu^2 = \delta_c^2/s$. (Strictly speaking, to compare most directly with Sheth et al. (2001) we should account for the distribution in $\delta_{\rm c}$ values at each s; but the constant deterministic $\delta_{\rm c}$ discussion below captures the gist of the argument. Also, our expressions below are appropriate for a sharp-k filter, but the logic, and so the qualitative trends, do not depend on this choice.)

In our ESP model, this fraction is given by taking each peak of mass M, then accounting for the distribution of excursion set predictions for $s(m) > S(M)$ which come from all the other mass elements which make up M (rather than just the one mass element at the center of mass), and integrating the distribution of S over the range $0 < S < s$. I.e.,

$$sf(s) = \int_0^s \frac{{\rm d}S}{S}\,Sf_{\rm ESP}(S)\,sf(s|S). \qquad (14)$$

where

$$Sf_{\rm ESP}(S) = \frac{M}{\bar\rho}\,\frac{{\rm d}n_{\rm ESP}(M)}{{\rm d}\ln M}\,\left|\frac{{\rm d}\ln M}{{\rm d}\ln S}\right| \qquad (15)$$

(from equation 2) and $f(s|S)$ is the excursion set prediction for the mass fraction of M which is incorrectly predicted to instead have mass $m = M(s)$ instead of $M(S)$. Because we know $sf(s)$ as well as $n_{\rm ESP}(S)$ we can solve (by numerical back substitution) for $f(s|S)$. However, we can get a simple, intuitive estimate of the result as follows.

For constant $\delta_{\rm c}$, Figures 1 and 2 in Paranjape & Sheth (2012) shows that $Sf_{\rm ESP}(S)$ is rather well-approximated simply by $\nu f(\nu) = \nu\,\exp(-\nu^2/2)/\sqrt{2\pi}$ with $\nu^2 = (\Xi\delta_c)^2/S$ for some $\Xi < 1$. (Strictly speaking, they used the Sheth-Tormen functional form for $\nu f(\nu)$; however, at high masses, this form reduces to the simpler one given here with $\Xi = \sqrt{0.7}$.) Since this is the same functional form for S that appears on the left hand side of equation (14) for s, it is easy to check that $sf(s|S)$ should also be the same function of ν, but with $\nu^2 = (\delta_c - \Xi\delta_c)^2/(s - S)$.

Thus, this calculation shows explicitly that the average over all walks will yield f which has a similar functional form to the one for the specially chosen subset, but the two will have different values of δ_c. Moreover, the distribution of predicted masses will be very different from a delta function centered on M. Rather, it will look just like the conditional excursion set prediction for the fraction of all walks which first cross $\delta_{\rm c}$ on scale s given that they are known to pass through $\Xi\delta_{\rm c} < \delta_{\rm c}$ on scale S before first crossing $\delta_{\rm c}$. This latter point quantifies the explanation given by Sheth et al. (2001) when addressing the concerns raised by White (1996). It also expands on a point first made by Paranjape & Sheth (2012): the ESP framework naturally accounts for the fact that one must rescale $\nu \to \sqrt{q}\nu$ with $q \sim 0.7$ if one wants to use the usual excursion set expressions (based on the statistics of all positions) to model halo counts – but this rescaling is not necessary if one uses the statistics of the special positions for which the physics is simplest. Of course, because the physics of collapse refers to collapse around the halo centers of masses, and not around random positions in space, this discussion highlights the dangers of interpreting the barrier height in the random walk calculation with that for the physics of collapse around special positions in space.

4 HALO BIAS

In this section we derive expressions for the predicted clustering of halos in our model.

The Lagrangian bias associated with excursion set peaks follows from writing the conditional mass function as discussed by Musso et al. (2012) and Paranjape & Sheth (2012). Introducing scatter in the barrier parameter β is straightforward, as we discuss below. The ESP conditional multiplicity function for a square-root barrier at fixed β *and* a fixed density δ_0 at scale S_0 is given by

$$f_{\rm ESP}(\nu|\beta,\delta_0) = (V/V_*)p(B/\sqrt{s}|\delta_0) \times \frac{1}{\gamma\nu}\int_{\beta\gamma}^{\infty} {\rm d}x\,(x-\beta\gamma)F(x) \times p(x|B/\sqrt{s},\delta_0)\,, \qquad (16)$$

where $p(\mu|\delta_0)$ and $p(x|\mu,\delta_0)$ are 1-dimensional conditional Gaussian distributions that can be written using the covariance matrix of the trivariate Gaussian in (μ, x, δ_0).

The arguments of Musso et al. (2012) show that the bias coefficients $\delta_{\rm c}^n b_n$ are the Taylor coefficients of the expansion of equation (16) in terms of $\bar\delta_0 = \delta_0/\delta_{\rm c}$, upon imposing the condition $\tilde{\mathbf{c}} = 0$, where $\tilde{\mathbf{c}}$ is the matrix that one must subtract from the unconditional covariance matrix of the variables (μ, x) to obtain the covariance matrix of the conditional Gaussian $p(\mu, x|\delta_0)$. The resulting conditional multiplicity is

$$\begin{aligned} f_{\rm ESP}(\nu|\beta,\delta_0,\tilde{\mathbf{c}}=0) &= (V/V_*)\left({\rm e}^{-(\nu+\beta-\bar\delta_0(S_\times/S_0)\nu)^2/2}/\sqrt{2\pi}\right) \\ &\times \frac{1}{\gamma\nu}\int_{\beta\gamma}^{\infty}{\rm d}x\,(x-\beta\gamma)F(x) \\ &\times p_{\rm G}(x-\beta\gamma-\gamma\nu_1;1-\gamma^2)\,, \qquad (17)\end{aligned}$$

where we have defined $\nu_1 \equiv \nu(1-\bar\delta_0(S_\times/S_0)(1-\epsilon_\times))$, and

$$\begin{aligned} S_\times &= \int {\rm d}\ln k\,\Delta^2(k)W(kR)W(kR_0)\,, \\ \epsilon_\times &= 2\,{\rm d}\ln S_\times/{\rm d}\ln s \qquad (18)\end{aligned}$$

are cross-correlations between the small and the large scale.

At fixed β, the bias parameters can be written as

$$\begin{aligned} \frac{\delta_{\rm c}b_1(\nu,\beta)}{(S_\times/S_0)} &= \mu_1(\nu,\beta) + (1-\epsilon_\times)\lambda_1(\nu,\beta)\,, \qquad (19) \\ \frac{\delta_{\rm c}^2 b_2(\nu,\beta)}{(S_\times/S_0)^2} &= \mu_2(\nu,\beta) + 2(1-\epsilon_\times)\mu_1(\nu,\beta)\lambda_1(\nu,\beta) \\ &+ (1-\epsilon_\times)^2\lambda_2(\nu,\beta)\,, \qquad (20)\end{aligned}$$

where, using $\Gamma \equiv \gamma/\sqrt{1-\gamma^2}$,

$$\begin{aligned} \mu_n(\nu,\beta) &= \nu^n H_n(\nu+\beta)\,, \qquad (21) \\ \lambda_n(\nu,\beta) &= (-\Gamma\nu)^n \left\langle H_n\,(y-\beta\Gamma-\Gamma\nu)|\,\nu,\beta\right\rangle_y\,, \qquad (22)\end{aligned}$$

where $H_n(x) = {\rm e}^{x^2/2}(-d/dx)^n{\rm e}^{-x^2/2}$ are the "probabilist's" Hermite polynomials, and for some function $h(y,\nu,\beta)$, we have

$$\left\langle h(y,\nu,\beta)|\nu,\beta\right\rangle_y = \frac{\int_{\beta\Gamma}^{\infty}{\rm d}y\,(y-\beta\Gamma)F(y\gamma/\Gamma)p_{\rm G}(y-\beta\Gamma-\Gamma\nu;1)h(y,\nu,\beta)}{\int_{\beta\Gamma}^{\infty}{\rm d}y\,(y-\beta\Gamma)F(y\gamma/\Gamma)p_{\rm G}(y-\beta\Gamma-\Gamma\nu;1)}\,. \qquad (23)$$

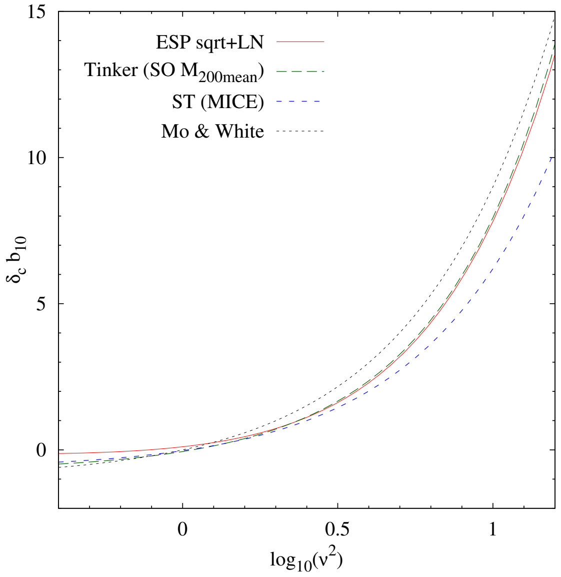

Figure 3. Scale-independent (peak-background split) linear Lagrangian halo bias $\delta_{\rm c}b_{10}$ in the ESP framework for a square-root barrier with Lognormal scatter (solid red). This curve is in excellent agreement with the fit to N-body simulations from Tinker et al. (2010), the simulations being the same as those for which Figure 2 showed a mass function comparison (see text for a discussion). The dotted black curve is the spherical collapse prediction ν^2-1 (Mo & White, 1996), and the short-dashed blue curve is the peak-background split prediction associated with the mass function fit to the MICE simulations.

Marginalising over β gives the bias parameters as

$$\begin{aligned} \delta_{\rm c}b_1(\nu) &= \left(\frac{S_\times}{S_0}\right)\Big[\langle\,\mu_1|\nu\,\rangle + (1-\epsilon_\times)\,\langle\,\lambda_1|\nu\,\rangle\Big]\,, \qquad (24) \\ \delta_{\rm c}^2 b_2(\nu) &= \left(\frac{S_\times}{S_0}\right)^2\Big[\langle\,\mu_2|\nu\,\rangle + 2(1-\epsilon_\times)\,\langle\,\mu_1\lambda_1|\nu\,\rangle \\ &+ (1-\epsilon_\times)^2\,\langle\,\lambda_2|\nu\,\rangle\Big]\,, \qquad (25)\end{aligned}$$

where, for some function $g(\nu,\beta)$, we have

$$\langle\,g|\nu\,\rangle = \frac{\int{\rm d}\beta\,p(\beta)f_{\rm ESP}(\nu|\beta)g(\nu,\beta)}{\int{\rm d}\beta\,p(\beta)f_{\rm ESP}(\nu|\beta)}\,. \qquad (26)$$

The presence of $\epsilon_\times$ in these expressions for real-space bias is an indication of k-dependent Fourier-space bias, as discussed at length by Musso et al. (2012).

Musso et al. (2012) also showed that the usual peak-background split expressions for bias (which they denoted as b_{n0}) correspond to taking the large scale limit $R_0 \to \infty$, or equivalently, setting $\epsilon_\times \to 0$ and $S_\times/S_0 \to 1$ in the coefficients b_n. Figure 3 shows our ESP prediction for the linear peak-background split bias $\delta_{\rm c}b_{10}$ (i.e., setting $\epsilon_\times = 0$, $S_\times/S_0 = 1$ in equation 24) as the solid red curve. The dotted black curve is the spherical collapse prediction ν^2-1 (Mo & White, 1996). The dashed green curve shows the fit presented by Tinker et al. (2010) for the same simulations analysed by Tinker et al. (2008). We have checked that in this case the results for the

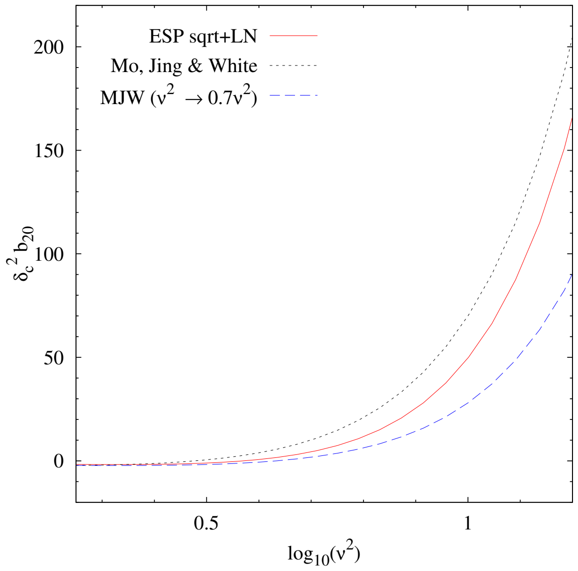

Figure 4. Same as previous Figure, but now for the second order bias coefficient. In this case, there are no measurements from simulations with which to compare.

WMAP1 and WMAP3 cosmologies are nearly identical, so we only show the results for WMAP3. The ESP curve matches the N-body fit very well at large masses, which is where the ESP framework is expected to work well. Note that the curve for Tinker et al. (2010) is not simply the logarithmic derivative of the mass function calibrated by Tinker et al. (2008); that derivative would underestimate the large scale bias by up to 10% (Manera et al., 2010; Tinker et al., 2010). (For comparison, the short-dashed blue curve shows the peak-background split prediction for the MICE mass function.)

Figure 4 shows the corresponding result for the quadratic peak-background split coefficient $\delta_{\rm c}^2 b_{20}$ for ESP (solid red) and the spherical collapse result $\nu^2(\nu^2-3)$ (Mo, Jing & White, 1997, dotted black). The dashed blue curve shows the Mo et al. (1997) expression after rescaling $\nu \to \sqrt{0.7}\nu$. In this case, there are no measurements in simulations with which to compare – this is the subject of ongoing work – but we have included the Figure to show that b_{20} behaves qualitatively like b_{10}, transitioning from the usual (sharp-k excursion set) expression rescaled by $\nu \to \sqrt{0.7}\nu$ at $\nu \sim 1$ to lying above this rescaled value at larger ν.

These plots illustrate another point made by Paranjape & Sheth (2012): the ESP framework naturally accounts for the fact that the measured large scale bias deviates from that predicted by a naive application of the peak-background split to a mass function that was fit using the rescaled variable $\nu \to \sqrt{q}\nu$ with $q \sim 0.7$.

4.1 Reconstructing the peak-background split parameters

In this subsection we revisit the idea of reconstructing the peak-background split parameters b_{n0} from suitable real-space measurements of the parameters b_n (Musso et al., 2012). In particular, we wish to address some subtleties that arise due to the stochasticity of the barrier height.

The theoretical quantities plotted in Figures 3 and 4 required us to set $\epsilon_\times \to 0$ and $S_\times/S_0 \to 1$ by hand. In Fourier space, this would correspond in practice to taking the limit $k \sim 1/R_0 \to 0$, which is how Tinker et al. (2010) e.g. derived their fit for the linear bias. Musso et al. (2012), on the other hand, pointed out that the theoretical predictions for $\delta_{\rm c}^n b_n$ at *finite* R_0 are equivalent to an average over the Hermite-transformed initial density field $H_n(\delta_0/\sqrt{S_0})$ at the centers of halos. To be precise, if there are N halos in a given mass bin, one estimates the bias parameters at this mass as

$$b_n^{(\rm msd)} = S_0^{-n/2}\,\frac{1}{N}\sum_{i=1}^{N} H_n(\delta_{0i}/\sqrt{S_0})\,, \qquad (27)$$

where δ_{0i} is the Lagrangian density contrast smoothed on scale R_0 and centered on the $i^{\rm th}$ halo in the bin, and S_0 is the linearly extrapolated variance at R_0.

If we use a deterministic barrier in our theoretical model for the bias, then these measurements can be explicitly converted into estimates of the peak-background split parameters b_{n0} (Musso et al., 2012; Paranjape & Sheth, 2012). To see this, note that for the square-root barrier with fixed β, we can use equations (19) and (20) to write the peak-background split parameters in terms of $b_1(\nu,\beta)$ and $b_2(\nu,\beta)$ as

$$\begin{aligned}
\delta_{\rm c} b_{10}(\nu,\beta) &= \mu_1 + \lambda_1 \\
&= \frac{1}{(1-\epsilon_\times)}\left[\frac{\delta_{\rm c} b_1(\nu,\beta)}{(S_\times/S_0)} - \epsilon_\times\mu_1\right], \qquad (28)\\
\delta_{\rm c}^2 b_{20}(\nu,\beta) &= \mu_2 + 2\mu_1\lambda_1 + \lambda_2 \\
&= \frac{1}{(1-\epsilon_\times)^2}\left[\frac{\delta_{\rm c}^2 b_2(\nu,\beta)}{(S_\times/S_0)^2}\right. \\
&\qquad - 2\epsilon_\times\mu_1\left(\frac{\delta_{\rm c} b_1(\nu,\beta)}{(S_\times/S_0)} - \mu_1\right) \\
&\qquad \left. - \epsilon_\times(2-\epsilon_\times)\mu_2\right], \qquad (29)
\end{aligned}$$

which reduce to the expressions in equations (44) and (47) of Musso et al. (2012) when $\beta = 0$.

If β is stochastic (as we have seen it must be), then the measurements on the r.h.s. of equation (27) correspond to the marginalised bias coefficients – $b_n^{(\rm msd)} \leftrightarrow \langle\, b_n(\nu,\beta)|\nu\,\rangle$ – since we did not keep track of the value of β for each halo. For the linear coefficient b_{10} this does not pose any problem, and we can estimate this coefficient using $\langle\,\mu_1|\nu\,\rangle$, which is calculable, and the measured linear bias,

$$\delta_{\rm c} b_{10}^{(\rm msd)}(\nu) = \frac{1}{(1-\epsilon_\times)}\left[\frac{\delta_{\rm c} b_1^{(\rm msd)}}{(S_\times/S_0)} - \epsilon_\times\,\langle\,\mu_1|\nu\,\rangle\right]. \qquad (30)$$

For b_{20}, however, we must deal with a term involving $\langle\, b_1(\nu,\beta)\mu_1(\nu,\beta)|\nu\,\rangle$. In practice, measuring this term would involve knowing the value of β for each halo. While this is do-able in an N-body simulation, it makes the reconstruction technique very cumbersome. In order to keep the algorithm simple, we will assume that this term can be split as $\langle\, b_1(\nu,\beta)\mu_1(\nu,\beta)|\nu\,\rangle = \langle\, b_1(\nu,\beta)|\nu\,\rangle\,\langle\, \mu_1(\nu,\beta)|\nu\,\rangle = b_1^{(\mathrm{msd})}\,\langle\, \mu_1|\nu\,\rangle$. This assumption can be explicitly tested using N-body simulations. With this caveat, the reconstructed quadratic coefficient is

$$\begin{aligned}\delta_{\mathrm{c}}^2 b_{20}^{(\mathrm{msd})}(\nu) = \frac{1}{(1-\epsilon_\times)^2}\Bigg[&\frac{\delta_{\mathrm{c}}^2 b_2^{(\mathrm{msd})}}{(S_\times/S_0)^2}\\ &- 2\epsilon_\times\left(\frac{\delta_{\mathrm{c}} b_1^{(\mathrm{msd})}}{(S_\times/S_0)}\,\langle\, \mu_1|\nu\,\rangle - \langle\, \mu_1^2|\nu\,\rangle\right)\\ &- \epsilon_\times(2-\epsilon_\times)\,\langle\, \mu_2|\nu\,\rangle\Bigg]\,.\end{aligned} \qquad (31)$$

The remaining averages over β simplify to some extent, and we have

$$\begin{aligned}\langle\, \mu_1|\nu\,\rangle &= \nu\,(\nu + \langle\, \beta|\nu\,\rangle)\,,\\ \langle\, \mu_2|\nu\,\rangle &= \langle\, \mu_1^2|\nu\,\rangle - \nu^2\\ &= \nu^2\left(\nu^2 - 1 - 2\nu\,\langle\, \beta|\nu\,\rangle + \langle\, \beta^2|\nu\,\rangle\right)\,,\end{aligned} \qquad (32)$$

with

$$\left\langle\, \beta^j|\nu\,\right\rangle = \frac{\int \mathrm{d}\beta\, p(\beta) f_{\mathrm{ESP}}(\nu|\beta)\beta^j}{\int \mathrm{d}\beta\, p(\beta) f_{\mathrm{ESP}}(\nu|\beta)}\,. \qquad (33)$$

5 DISCUSSION

We have presented a derivation of equation (12), which represents the first analytic model of halo abundances which accounts self-consistently for the fact that the physics of collapse is best described around the halo center of mass, is not spherical, and can vary substantially from one place in the universe to another. The comparison between equation (12) and halo counts in simulations (Figure 2) is very encouraging. (Figure 1 shows that accounting for the physics of non-spherical collapse is necessary.)

We also derived expressions for the associated large scale bias factors b_{10} and b_{20} (these follow from setting $\epsilon_\times \to 0$ and $S_\times/S_0 \to 1$ in equations 24 and 25); the former is in very good agreement with measurements from simulations. We are in the process of determining if b_{20} is similarly accurate. Additionally, we showed how real-space measurements of b_1 and b_2 can be converted to practical estimates of b_{10} and b_{20} (equations 30 and 31), which extends the results of Musso et al. (2012) and Paranjape & Sheth (2012) to the case of stochastic barrier heights. Testing the accuracy of this reconstruction in N-body simulations is also work in progress.

Our ESP analysis highlighted the benefits of developing a model for the abundance of positions in space around which the physics of collapse is simplest. In Section 3, we showed that it can be used to understand what would have happened if one had instead studied all initial positions. This provides the basis for a number of other tests of the more formal aspects of our approach – as well as elucidating the relation between our ESP calculation and the usual excursion set approach.

Our model has no free parameters, although it must take as input one physical quantity from simulations. This quantity describes how the typical density required for collapse depends on proto-halo mass, and how much this density varies from one proto-halo to the next. While the triaxial collapse model correctly predicts that this mean value and the scatter around it should increase as halo mass decreases, the predicted scatter is smaller than observed. We therefore hope that our work will motivate studies of the physical origin of $p(\beta)$. One obvious direction here is that peaks have non-trivial deformation *and* inertia tensors. Non-spherical initial shapes mean the critical density for collapse will now depend not just on the tidal field but on the shape and the misalignment angle between the principal axes of the two tensors. In principle, our ESP model contains a prescription for the distribution of shapes (and misalignments) for which one should run the ellipsoidal collapse model.

Futhermore, we do not expect our model to apply at masses for which $\delta_{\mathrm{c}}(m)/\sigma_0(m) < 1$, as there is no physically compelling reason why a peak of (normalized) height 1 should dominate its surroundings. While this mass regime may be less interesting for studies which use the abundance of rich clusters to constrain cosmological models, understanding it is useful for understanding the formation and evolution of galaxies. So we hope our approach of identifying just what it is that is special about the positions around which gravitational collapse occurs, and then using only these positions to make inferences about halo assembly histories, will eventually provide insight into the low mass regime as well.

ACKNOWLEDGEMENTS

We thank Christophe Pichon for discussions, and for pointing out to us the work of Hanami (2001). This work is supported in part by NSF-0908241 and NASA NNX11A125G (RKS, AP), and by the Swiss National Science Foundation (VD). AP thanks A. Réfrégier and A. Amara at ETH, Zürich for hospitality during a visit when this work was completed. VD also wishes to thank ICTP for hospitality when parts of this work were completed.

References

Appel L., Jones B. J. T., 1990, MNRAS, 245, 522

Bardeen J. M., Bond J. R., Kaiser N., Szalay A. S., 1986, ApJ, 304, 15

Bond J. R., Cole S., Efstathiou G., Kaiser N., 1991, ApJ, 379, 440

Bond J. R., Myers S. T., 1996, ApJS, 103, 1
Chiueh T., Lee J., 2001, ApJ, 558, 83
Corasaniti P. S., Achitouv I., 2011, PRL, 106, 241302
Crocce M., Fosalba P., Castander F. J., Gaztañaga E., 2010, MNRAS, 403, 1353
Dalal N., White M., Bond J. R., Shirokov A., 2008, ApJ, 687, 12
Desjacques V., 2008, MNRAS, 388, 638
Desjacques V., Sheth R. K., 2010, PRD, 81, 023526
Elia A., Ludlow A. D., Porciani C., 2012, MNRAS, 421, 3472
Hanami H., 2001, MNRAS, 327, 721
Ludlow A. D., Porciani C., 2011, MNRAS, 413, 1961
Maggiore M., Riotto A., 2010, ApJ, 711, 907
Maggiore M., Riotto A., 2010, ApJ, 717, 515
Manera M., Scoccimarro R., Sheth R. K., 2010, MNRAS, 402, 589
Manrique A., Raig A., Solanes J. A., González-Casado G., Stein P., Salvador-Solé, 1998, ApJ, 499, 548
Mo H. J, Jing Y. P., White S. D. M., 1997, MNRAS, 284, 189
Mo H. J., White S. D. M., 1996, MNRAS, 282, 347
Musso M., Paranjape A., Sheth R. K., 2012, MNRAS, accepted, arXiv:1205.3401
Musso M., Sheth R. K., 2012, MNRAS, 423, 102
Paranjape A., Lam T.-Y., Sheth R. K., 2012, MNRAS, 420, 1429
Paranjape A., Sheth R. K., 2012, MNRAS, accepted, arXiv:1206.3506
Peacock J. A., Heavens A. F., 1990, MNRAS, 243, 133
Press W. H., Schechter P., 1974, ApJ, 187, 425
Robertson B. E., Kravtsov A. V., Tinker J., Zentner A. R, 2009, ApJ, 696, 636
Sheth R. K., 2009, AIP Conf. Proc., 1132, 158
Sheth R. K., 2011, Pramana, 77, 169
Sheth R. K., Chan K. C., Scoccimarro R., 2012, arXiv:1207.7117
Sheth R. K., Mo H. J., Tormen G., 2001, MNRAS, 323, 1
Sheth R. K., Tormen G., 1999, MNRAS, 308, 119
Sheth R. K., Tormen G., 2002, MNRAS, 329, 61
Tinker J. L., Kravtsov A. V., Klypin A., Abazajian K., Warren M. S., Yepes G., Gottlöber S., Holz D. E., 2008, ApJ, 688, 709
Tinker J. L., Robertson B. E., Kravtsov A. V., Klypin A., Warren M. S., Yepes G., Gottlöber S., 2010, ApJ, 724, 878
White S. D. M., 1996, in Schaeffer R. et al., eds., Cosmology and large scale structure, Proc. 60th Les Houches School, ASP Conf. Series, Vol. 176. Elsevier, Amsterdam, p. 349